Nanoconstruction of Microspheres and Microcapsules Using Proton-Induced Phase Transitions: Molecular Self-Recognition by Diamide Diacids in Water

O. Phanstiel IV,*,† R. J. Lachicotte,‡ D. Torres,§ M. Richardson,§ H. Matsui,† H. Schaffer,|| F. Adar,|| J. Liu,⊥ and D. Seconi†

Center for Discovery of Drugs and Diagnostics, Department of Chemistry, and Center for Research and Education in Optics and Lasers, University of Central Florida, Orlando, Florida 32816, Department of Chemistry, University of Rochester, Rochester, New York 14627, Instrument SA, Metuchen, New Jersey 08840, and Institute of Molecular Biophysics, Florida State University, Tallahassee, Florida 32306

Received August 15, 2000. Revised Manuscript Received October 20, 2000

Bis(N^{α}-amido-L-phenylalanine)-1,1-cyclobutane dicarboxylate (**5**) was studied by Fourier transform infrared (FTIR) spectroscopy, variable-temperature NMR (VT-NMR), transmission electron microscopy, X-ray crystallography, Raman microscopy, and a novel imaging technique known as "soft" X-ray microscopy (XRM). Diamide diacid **5** was shown to self-associate into solid microspheres during a proton-induced phase transition from the solvated state to the desolvated assembled state. These diverse techniques allowed for the delineation of the molecular recognition events involved in the assembly process. X-ray crystallography revealed that **5** packs in a bundled helical array comprised of two types of intermolecular hydrogen bonds (i.e., OC═O···HN and COOH···O═CN). VT-NMR and IR measurements of **5** (1 mM in $CDCl_3$) revealed the small temperature dependence of the amide NH chemical shift ($\Delta\delta/\Delta T = -1.1$ ppb/K) and the availability of the "free" amide NH of **5** to form intermolecular hydrogen bonds. Supramolecular rodlike structures were observed during the aqueous assembly of **5** into microspheres by XRM. Raman microscopy confirmed that nearly identical bonding patterns are present in the assembled microsphere and the crystal architecture of **5**. Collectively, these observations provide compelling evidence that the assembly of **5** occurs via crystalline supramolecular intermediates, which are similar in shape and have complementary bonding motifs for proper self-recognition. Competition experiments involving varying concentrations of **5** and its microcapsule-forming cyclopropane analogue **3** revealed that molecular fidelity was less important to the microsphere-forming process than the related capsule-forming process.

Introduction

Protein folding, peptide agglomeration, and peptide self-replication processes all involve molecular recognition events.[1−3] Understanding which biophysical factors are responsible for the molecular ordering of model amides may lead to new insights into how proteins recognize other peptides in vivo.[4] This information could then be applied to the design of templated systems, which self-organize in aqueous environments.[3,5−7] The ability to control specific noncovalent interactions between small amide systems in water is clearly a formidable challenge. Nevertheless, low-molecular-weight, "smart" molecules have been designed which contain molecular recognition information and are capable of constructing supramolecular architectures in aqueous environments.[5−7]

A proton-induced phase (PIP) transition has been shown to order small building blocks into larger constructs. When the pH of the water phase is lowered, soluble carboxylate salts are converted into their insoluble carboxylic acid motifs. This transition usually results in the formation of crystals or an amorphous solid being produced. However, certain architectures have been shown to generate supramolecular constructs such as microcapsules and microspheres.[5−7] In this report 1,1-cyclobutane-containing diamide diacids are shown to self-associate into microspheres in the presence of water.

† Center for Discovery of Drugs and Diagnostics, Department of Chemistry, University of Central Florida.
‡ University of Rochester.
§ Center for Research and Education in Optics and Lasers, University of Central Florida.
|| Instrument SA.
⊥ Florida State University.

(1) Albert, J. S.; Goodman, M. S.; Hamilton, A. D. *J. Am. Chem. Soc.* **1995**, *117*, 1143−1144.
(2) Rebek, J., Jr.; Williams, K. *J. Am. Chem. Soc.* **1987**, *109*, 5033−5035 and references therein.
(3) Lee, D. H.; Granja, J. R.; Martinez, J. A.; Severin, K.; Ghadiri, M. R. *Nature* **1996**, *382*, 525.
(4) Appella, D. H.; Barchi, J. J., Jr.; Durell, S. R.; Gellman, S. H. *J. Am. Chem. Soc.* **1999**, *121*, 2309−2310.
(5) Bergeron, R. J.; Phanstiel, O., IV; Yao, G. W.; Milstein, S.; Weimar, W. R. *J. Am. Chem. Soc.* **1994**, *116*, 8479−8484.
(6) Bergeron, R. J.; Yao, G. W.; Erdos, G. W.; Milstein, S.; Gao, F.; Weimar, W. R.; Phanstiel, O., IV. *J. Am. Chem. Soc.* **1995**, *117*, 6658−6665.
(7) Bergeron, R. J.; Yao, G. W.; Erdos, G. W.; Milstein, S.; Gao, F.; Rocca, J.; Weimar, W. R.; Price, H. L.; Phanstiel, O., IV. *Bioorg. Med. Chem.* **1997**, *5*, 2049−2061.

10.1021/cm0006547 CCC: $20.00
Published on Web 01/10/2001

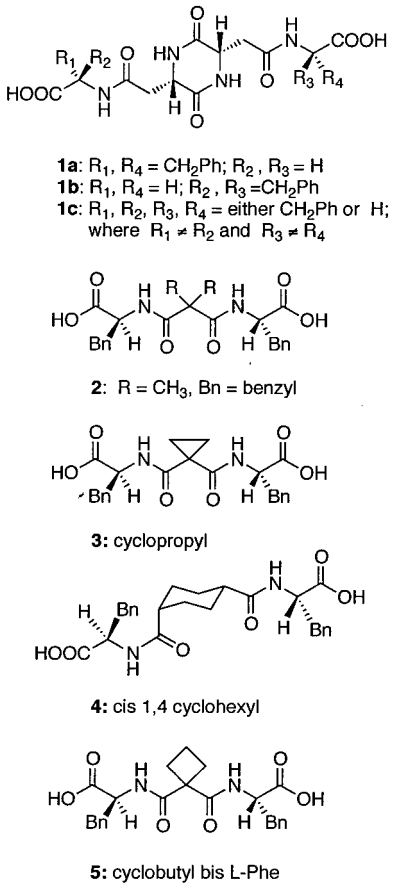

Figure 1. Self-assembling diacid derivatives.

Earlier structure−activity studies revealed that this self-organizing process was restricted to systems containing certain aromatic amino acids (e.g., **1a**−**c**, **2a**−**c**, **3**, and **4** in Figure 1).[5−7] In general, these systems are comprised of two L-phenylalanine (L-Phe) groups appended via N^{α}-amide bonds to an organic spacer group or "platform" (see Figure 1). Although the precise intermolecular packing arrangement was unknown, both the spacer distance and the conformational mobility of the platform were shown to influence the type of self-assembly observed.[6,7] Prior work revealed that, upon a pH adjustment, the cyclopropyl diamide diacid **3** assembled into microcapsules, whereas the *cis*-1,4-cyclohexylene derivative **4** generated a suspension of solid microspheres.[6,7] Intrigued by this observation, we were interested in whether small perturbations in the platform architecture of **3** could convert the capsule-generating process into one that created microspheres. Because a dynamic ring-flip process was expected in the platform of **4**,[7] the 1,1-disubstituted cyclobutane platform was selected for study because it represents the smallest cycloalkane with marginal ring-puckering abilities. In addition, the ring expansion (in going from **3** to **5**) was expected to impart subtle angular differences in ϕ [the (O)C−C−C(O) bond angle] while keeping the distance of the tether fixed. Remarkably, this minor platform alteration changed the assembly outcome from microcapsules (with **3**) to microspheres (with **5**). To better understand this observation, a detailed study of **5** was initiated using Fourier transform infrared (FTIR), variable-temperature NMR (VT-NMR), transmission electron microscopy (TEM), X-ray crystallography, Raman microscopy, and a novel imaging technique known as "soft" X-ray microscopy (XRM).[8] These diverse techniques have now provided the evidence necessary to formulate a mechanism by which these systems generate microspheres in aqueous environments. Such insights are an important first step in the design of future systems.

Scheme 1[a]

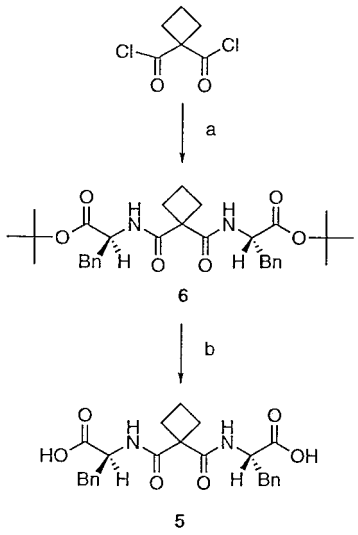

[a] Reagents: (a) L-phenylalanine *tert*-butyl ester (DIEA); (b) 40% TFA (by volume) in $CHCl_3$.

Results and Discussion

Synthesis. 1,1-Cyclobutanedicarboxylic acid was converted to its diacid chloride with excess thionyl chloride. As shown in Scheme 1, the diacid chloride was then condensed with 2 equiv of L-phenylalanine *tert*-butyl ester to give the diamide bis(*tert*-butyl) ester **6** (50% yield). Diester **6** was deprotected using trifluoroacetic acid (TFA) at room temperature to give the pure bis(L-phenylalanine) diamide diacid **5** in 31% yield after recrystallization from 50% hexane/ethyl acetate. The cyclopropyl derivative **3** was prepared by published methods for TEM comparison.[6] To generate the microsphere or microcapsule motifs, the diamide diacid was first dissolved in an aqueous base. The PIP transition was then triggered by the addition of aqueous citric acid (see the Experimental Section).

Transmission Electron Microscopy (TEM). Microassemblies generated from **3** and **5** were observed by TEM. The TEM technique allows one to discern whether hollow microcapsules or solid microspheres were formed. Solid motifs, such as the microspheres generated from **5**, lack an internal shell morphology and resemble hemispheres by TEM (Figure 2, panel A). In contrast, the microcapsule architectures generated from **3** have clearly defined shells contained within their spherical shape (Figure 2, panel B). To gauge the sensitivity of each self-assembly process, mixtures containing varying concentrations of the sodium salts

(8) (a) Richardson, M.; Torres, D.; De Priest, C.; Jin, F.; Shimkaveg, G. *Opt. Commun.* **1998**, *145*, 109−112. (b) Rajyaguru, J. M.; Kado, M.; Torres, D.; Richardson, M.; Muszynski, M. J. X-ray Microscopy and Imaging of *Escherichia coli*, LPS and DNA. *J. Microsc.* **1997**, *188*, 96−105.

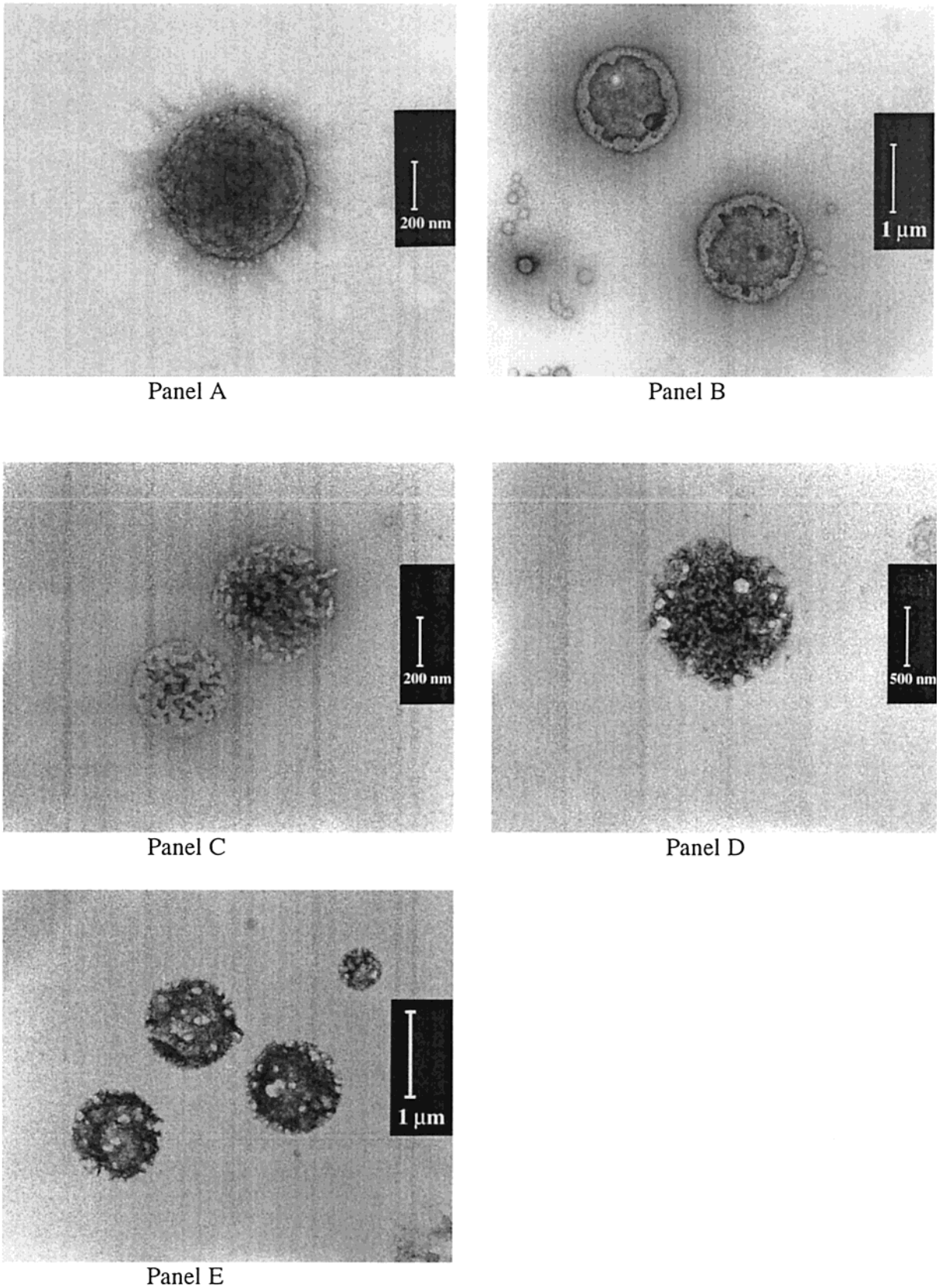

Figure 2. TEM images of microspheres and microcapsules generated from the following samples and mixtures: panel A, 100% **5**; panel B, 100% **3**; panel C, 75 mol % **5** and 25 mol % **3**; panel D, 25 mol % **5** and 75 mol % **3**; panel E: 50 mol % **5** and 50 mol % **3**.

of both substrates **3** and **5** were acidified with aqueous citric acid (see the Experimental Section). The results were imaged by TEM and are shown in Figure 2 (panels C−E). Inspection of Figure 2 provides several insights. First, the 50−50 mixture of **3** and **5** (panel E) generated a homogeneous population of microspheres. If the two self-assembly processes worked independently, one may have expected discreet colonies of microspheres and

microcapsules. This was not the case because only microspheres were observed. Panels C and D in Figure 2 suggest that the diacid **5** not only can accommodate the presence of cyclopropyl derivative **3** as it forms the microsphere motif but may actually incorporate **3** within its morphology. This form of "molecular infidelity" is highlighted by the observation (panel D) that derivative **5** at 25 mol % can direct the assembly outcome even in the presence of 75 mol % **3**. A corollary of these findings is that the microcapsule-generating process seems to be sensitive to the presence of other diamides of similar structure like **5** (e.g., 25 mol % **5** was sufficient to abort capsule formation by **3**, panel D).

X-ray Crystallography Data. Because this association process involves a phase transition into a solid array, we were interested in identifying the intermolecular contacts formed by **5** in the solid state. The ORTEP diagram is shown in Figure 3, panel A.

The dihedral angle defined by the four atoms of the cyclobutane ring (C11−C12−C13−C14 as numbered in Figure 3, panel A) reveals the expected deviation from planarity (16°) by the ring system. In addition, there are other geometric features which are noteworthy. First, the exocyclic (C15−C11−C10) bond angle ϕ is only 107°, while its complementary angle θ (C12−C11−C14) is 88.1°. C11 accommodates this geometry by slight elongation of the C11−C12 and C11−C14 bonds (1.56 and 1.55 Å, respectively) and expansion of the C10−C11−C14 and C15−C11−C12 bond angles (121.2° and 113.4°, respectively). Second, a consequence of this spatial arrrangement is that the appended amide carbonyls are oriented away from the puckered cyclobutane ring (presumably because of 1,3-diaxial interactions with the syn hydrogen on C13). Of particular interest is the fact that the carboxamides prefer a "diametrically opposed" orientation of the carbonyls at C10 and C15. This arrangement is evidenced by the dihedral angles: O3−C10−C11−C15 (80.5°) and C10−C11−C15−O4 (103.7°). To orient the reader, if one draws a vector along the dipole of the amide carbonyl (C→O), then these vectors point in nearly opposite directions in Figure 3. This orientation imparts a twist in the molecule, creating a staggered helical array of hydrogen bond donors and acceptors (see Figure 4), which act as recognition elements in the intermolecular packing of **5** in the solid state.

Inspection of the supramolecular packing of **5** in the solid state revealed the formation of extended helical arrays (Figure 3, panels B and C). These extended motifs are "stitched" together via a network of two types of intermolecular hydrogen bonds. Using Figures 3 and 4, one can clearly see that there are two complementary "docking" sites represented by the N2−H and C10−O3 pairs and their counterparts at N1−H and C15−O4, respectively. Within each pair, the NH and C═O bonds are oriented syn to each other. The first type of hydrogen bond involves a C═O···H−N bond, which connects the carboxylic acid carbonyl (e.g., C1−O2) of one molecule of **5** to the amide NH (O2···N2A; 3.302 Å) of a symmetry-related molecule. Similarly, the second hydrogen bond involves a O−H···O═C bond, which connects the carboxylic acid OH group (e.g., C1−O1−H) to the amide carbonyl (O1···O3A; 2.603 Å) of a symmetry-related molecule. These bonding patterns are present with the other pair at N1−H and C15−O4 and have intermolecular hydrogen bond interactions involving N1···O5A (2.954 Å) and O4···O6A (2.579 Å), respectively.

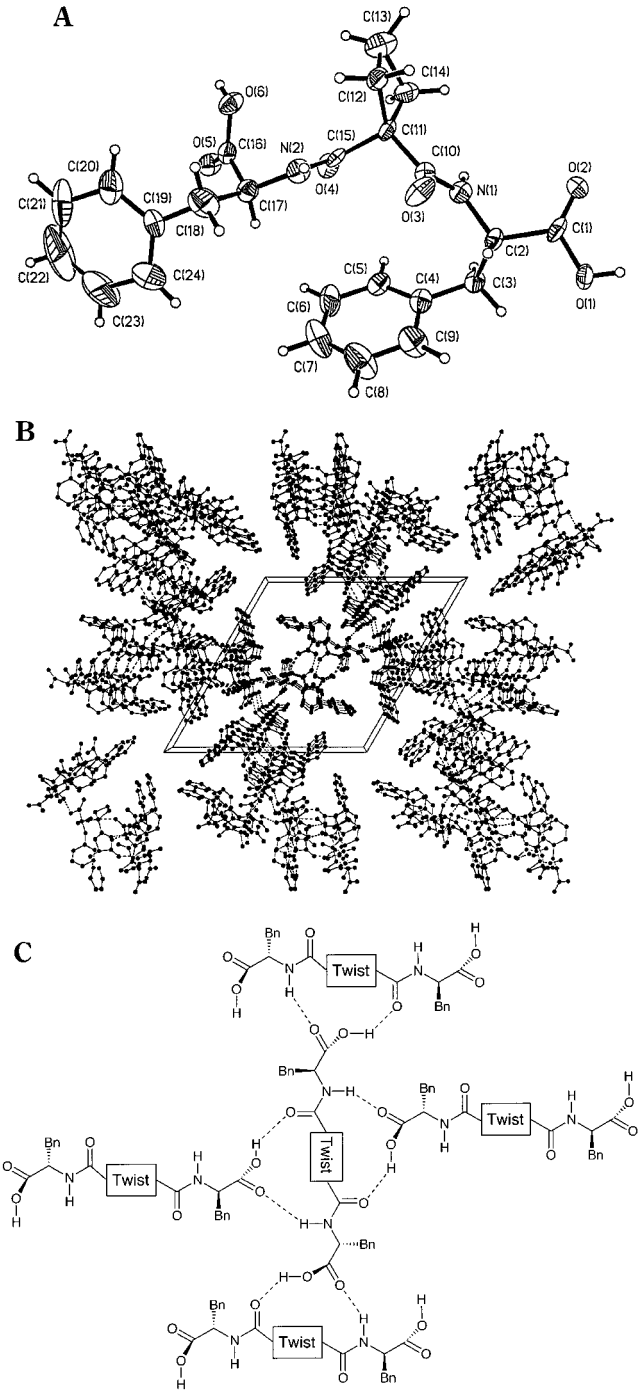

Figure 3. X-ray crystallography data. Panel A (top): ORTEP representation of **5**. Note: within the crystal studied there were two disordered sites. The preferred form (60%) is shown. The other population (40%) contained an alternative position of the phenyl ring and is provided as Supporting Information. Panel B (middle): crystalline array of **5**. Panel C (bottom): detailed image showing a hydrogen-bonding motif present in crystalline **5**.

In a recent theoretical description, Guo and Karplus suggested that the strength of the amide−amide−hydrogen bond is enhanced if both the carbonyl group and the NH group have hydrogen-bonding partners.[9]

(9) Guo, H.; Karplus, M. *J. Phys. Chem.* **1994**, *98*, 7104−7105.

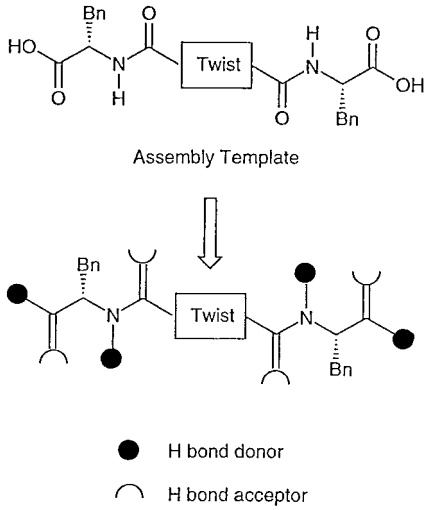

Figure 4. Staggered hydrogen-bonding array in **5.**

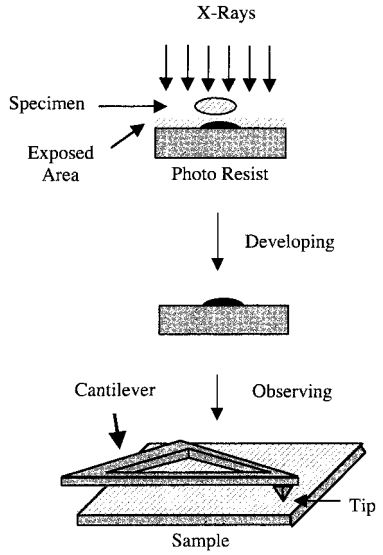

Figure 5. XRM imaging process.

Furthermore, Gung has suggested that such hydrogen-bonding "cooperativity" plays an important role in stabilizing helical conformations.[10] The crystal structure of **5** provides a striking example of these "cooperativity" effects wherein both the amide carbonyl and NH are involved in "cooperative" hydrogen bonds to form the extended crystalline array.

Intrigued by the behavior of **5** in the solid state, we speculated that these bundled motifs may be involved during the aqueous assembly of **5**[3,11−14] because the PIP transition returns **5** to its solid state. To address this premise, we looked for similar bundled morphologies (i.e., large rods) during the aqueous assembly of **5** using a novel imaging technique, XRM, and studied **5** by Raman microscopy, VT-NMR, and FTIR.

XRM. XRM provided an image of assembling constructs of **5** during their phase transition event in water. Because of the fast sampling time (<5 ns) of XRM, an instantaneous snapshot of **5** was captured as it assembled in an aqueous citric acid solution. Figure 5 illustrates the novel imaging process.

A single laser pulse (5 ns) generated "soft" X-rays (λ < 20 Å) from a gold foil target, which were then passed through an aqueous suspension of freshly generated microassemblies from **5**. At the border between the UV and X-ray regions of the electromagnetic spectrum (also known as the "water window"), organic molecules absorb radiation (λ < 20 Å) more strongly than water. The absorptivity differences (between organic molecules and water) are large enough that the water matrix is relatively transparent to these wavelengths.[8] The "soft" X-rays pass through a thin film (20 μm thick) of the aqueous suspension, are partially absorbed by the suspended organic assemblies, and impact a poly(methyl methacrylate) (PMMA) photoresist with reduced intensity. Conversely, if little organic matter is encountered, the soft "X-rays" strike the photoresist with full intensity and "soften" the polymer (via radiation-induced damage). Because this technique measures relative absorption by the PMMA resist over a fixed path length (20 μm), the location of the assemblies (near or far away from the surface of the resist) does not perturb the imaging method. The softened portions of the resist polymer are dissolved away (i.e., the resist is developed), and the remaining surface is imaged using an atomic force microscope (AFM). Because a relief image is generated, solid microspheres are observed as a collection of hemispheres on the photoresist surface (Figure 6, panel A).

There are several advantages to this technique. XRM provides the ability to image the assembly process as it takes place in an aqueous environment, with no further sample manipulation and, unlike SEM, without the use of high vacuum.[8] Moreover, the drying step required with SEM sample preparation may actually preclude the detection of supramolecular intermediates (rods), which likely coalesce upon concentration of the suspension.

AFM imaging of different regions of the PMMA resist surface revealed subpopulations, which appeared to be at different stages of the assembly process. Because of time constraints, one cannot image the entire surface but randomly selects different areas. In the case of **5,** the majority of the surface resembled the end product, a collection of microspheres (Figure 6, panel A). However, some regions were found to contain microspheres which appear to be under construction.

As shown in panel B of Figure 6, "wormlike" rods are clearly generated during the assembly of microspheres from **5** and appear to bundle together within a developing microsphere's core. It is not clear at this time

(10) Gung, B. W.; Zhu, Z.; Zou, D.; Everingham, B.; Oyeamalu, A.; Crist, R. M.; Baudlier, J. *J. Org. Chem.* **1998**, *63*, 5750−5761 and references therein.

(11) (a) Ghadiri, M. R.; Soares, C.; Choi, C. *J. Am. Chem. Soc.* **1992**, *114*, 825−831. (b) Kemp, D. S.; Allen, T. J.; Oslick, S. L. *J. Am. Chem. Soc.* **1995**, *117*, 6641−6657 and references therein.

(12) (a) Mutter, M.; Tuchscherer, G. G.; Miller, C.; Altmann, K.-H.; Carey, R. I.; Wyss, D. F.; Labhardt, A. M.; Rivier, J. E. *J. Am. Chem. Soc.* **1992**, *114*, 1463−1470. (b) Hecht, M. H.; Richardson, J. S.; Richardson, D. C.; Ogden, R. C. *Science* **1990**, *249*, 884−891.

(13) (a) Bolamphiphiles-forming helices: Furhop, J. H.; Demoulin, C.; Rosenberg, J.; Boettcher, C. *J. Am. Chem. Soc.* **1990**, *112*, 2827−2829. (b) Shimizu, T.; Mori, M.; Minamikawa, H.; Hato, M. *J. Chem. Soc., Chem. Commun.* **1990**, 183−185. (c) Shimizu, T.; Masuda, M. *J. Am. Chem. Soc.* **1997**, *119*, 2812−2818 and references therein. (d) Kogiso, M.; Ohnishi, S.; Yase, K.; Masuda, M.; Shimizu, T. *Langmuir* **1998**, 4978−4986 and references therein.

(14) For related findings with nanotubes: (a) Ghadiri, M. R.; Granja, J. R.; Milligan, R. A.; McRee, D. E.; Khazanovich, N. *Nature* **1993**, *366*, 324−327. (b) Ghadiri, M. R.; Granja, J. R.; Buehler, L. K. *Nature* **1994**, *369*, 301−304.

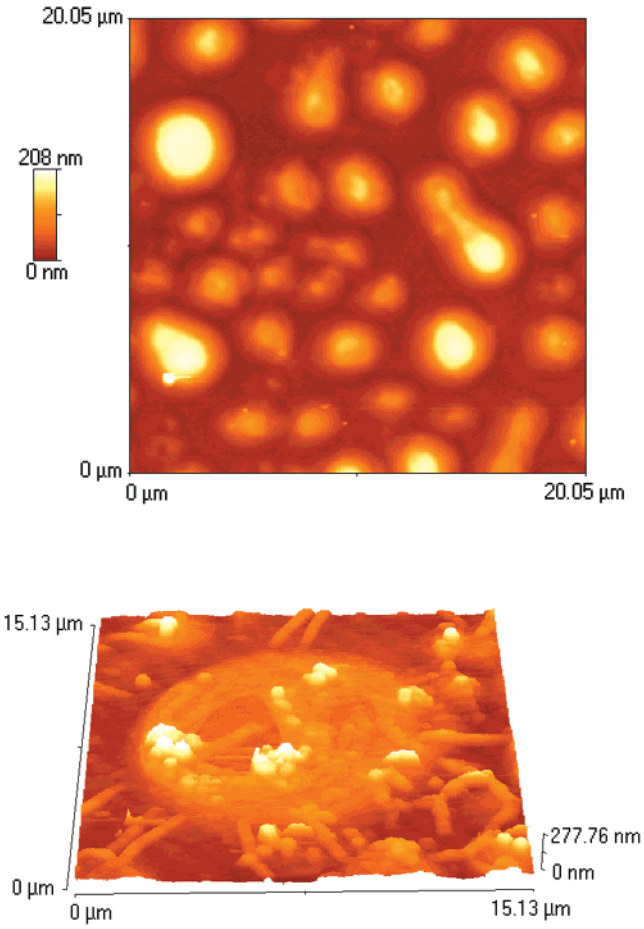

Figure 6. XRM images of nanoconstructs obtained with **5** and aqueous citric acid. Panel A (top): intact microspheres. Panel B (bottom): microsphere under construction via rodlike intermediates.

whether the rods are the supramolecular intermediates responsible for the microsphere's nanoconstruction or may be the result of an alternative aggregation pathway which is surface induced. Nevertheless, similar rodlike motifs have been observed with dicarboxylic oligopeptide bolaamphiphiles by Shimizu et al.[13d] In addition, there have been several papers describing template-assisted and metal-ion-assisted spontaneous self-assembly of polypeptides into helices[11] and helical bundles,[12] as well as the generation of helices from different types of bolaamphiphiles.[13] To the best of our knowledge, this is the first illustrated example of how low-molecular-weight diamide diacid systems may combine constructively to form the observed microsphere architectures.[6,7,14]

Unlike the famous "rope trick" involved in the interfacial polymerization of nylon 6,6,[15] this technology involves the formation of noncovalent interactions to generate larger structures. Because the bonding processes are reversible, a consequence of noncovalent construction is that the assembled architectures can be disassembled under certain conditions. In the case of both **3** and **5**, the suspended assemblies can be redissolved in water by an increase in the pH or by dilution.[16] In fact, several cycles of "nanoconstruction" and disassembly have been performed. Because the assembled architectures are not robust (i.e., they can aggregate into clusters of spheres), their isolation (by centrifugation or filtration) is problematic. Therefore, the microspheres are best studied as dilute suspensions (e.g., 10−25 mM) in aqueous citric acid (0.5 M).

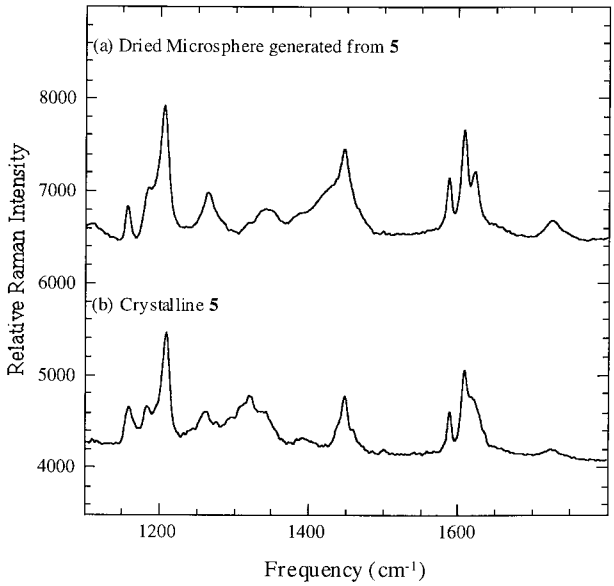

Figure 7. Raman microscopy studies.[18]

Raman Microscopy. Raman microscopy can be used to study liquids, crystalline solids, or amorphous samples.[17] One advantage of Raman microscopy is that via the collection of Raman scattering information one can attain a spatial resolution on the order of a few cubic microns. Because the microspheres generated from **5** typically range from submicron to approximately 5 μm in diameter, this resolution was sufficient to collect vibrational information from an immobilized single microsphere.[18] As shown in Figure 7, the Raman spectrum of crystalline **5** was nearly identical with that obtained from a microsphere (see the Experimental Section). Both spectra have the same features in terms of vibrational frequencies, peak intensity ratios, and peak shapes. These observations are consistent with the two samples having the same types of bonds, and the numbers of these bonds per area are approximately equal. A comparison of the two Raman spectra illustrated in Figure 7 supports a high degree of crystallinity in the assembled microsphere (see IR details below). Raman spectra of the nonmicrosphere-containing regions matched that of an aqueous citric acid/sodium carbonate solution sans **5** (see the Supporting Information). Because the assembled architecture seems to mirror the crystal morphology and the background mirrors that of the solvent, the Raman results are consistent with the expulsion of water from the as-

(15) Nylon rope trick: Pavia, D. L.; Lampman, G. M.; Kriz, G. S. *Introduction to Organic Laboratory Techniques*; Harcourt Brace College Publishers: Orlando, FL, 1988; pp 415−417.

(16) The assembly properties are concentration dependent and highly dependent on the structure of the diamide used, see refs 6 and 7.

(17) Turrell, G.; Corset, J. *Raman Microscopy: Developments and Applications*; Academic Press: New York, 1996.

(18) Raman spectra of the nonmicrosphere-containing regions, i.e., the surrounding area, matched that of a dried control solution containing equal volumes of 1 M aqueous citric acid and 50 mM aqueous sodium carbonate in the absence of **5**. For further details, see: Matsui, H.; Gologan, B.; Schaffer, H.; Adar, F.; Seconi, D.; Phanstiel, O., IV. *Langmuir* **2000**, *16*, 3148−3153.

sembly environment during the desolvation (i.e., the phase-transition) event. Taken together, the crystal and the Raman data provide strong evidence that crystalline architectures are, indeed, involved in the aqueous assembly process.[18]

^{1}H NMR and IR Studies. Acting as both a hydrogen bond donor and acceptor, water may interfere with the noncovalent assembly of **5** by competing effectively for hydrogen-bonding sites on **5**. This competitive solvation process makes both IR and NMR spectral interpretation of hydrophobic amide samples suspended in water difficult. These issues are compounded by the limited solubility of these systems in water. For these reasons, amide self-recognition studies are traditionally performed in anhydrous aprotic solvents (e.g., dichloromethane or chloroform), which do not competitively hydrogen bond with the substrates being examined.[10,19] VT-NMR and IR measurements are then used in tandem to delineate which specific inter- and intramolecular hydrogen bonds are established during the association process of the peptide (or polyamide) under study.[10]

In an attempt to explain the amide bonding preferences of **5**, the temperature dependence of the amide NH chemical shift of **5** (1 mM in $CDCl_3$) was determined to be −1.1 ppb/K. Because the NMR time scale is relatively slow, one observes a time average of the NH populations which are present. A small absolute value in ppb/K (∼1−2 ppb/K) denotes little change in the NH environment over this temperature range and is consistent with a solvent-exposed or "free" NH.[7,19,20] Therefore, the NMR studies demonstrated that the predominant NH population is solvent-exposed and not involved in intramolecular hydrogen bonds.

By inspecting these materials under dilute conditions (e.g., 1 mM), where intramolecular effects should be maximal, one can quantitate the innate availability of the amide NH for establishing intermolecular contacts at higher concentrations. In contrast to NMR, the faster time scale of FTIR allows one to observe the discreet NH populations in play. For example, with cyclobutyl derivative **5** (1 mM in CH_2Cl_2) we were able to compare the area under the absorption bands at 3405 (free NH, 60%) and 3329 cm^{-1} (intramolecularly bound NH, 40%), respectively. Note: the carbonyls for the COOH and amide groups were at 1724 and 1672 cm^{-1} (with another amide shoulder at 1640 cm^{-1}), respectively. These findings confirmed that, at least in CH_2Cl_2, **5** preferred not to form intramolecular bonds but to orient its NH's toward the solvent. These "solvent-exposed" or free NH's are thus available to form intermolecular contacts at higher concentrations. The FTIR results are consistent with the molecular twist present in the solid state of **5** (Figure 3) and the VT-NMR findings obtained in $CHCl_3$. At 10 and 100 mM **5** (in CH_2Cl_2), a new NH population at 3311 cm^{-1} and a new amide C═O at 1636 cm^{-1} were observed and are indicative of intermolecular hydrogen-bonded NH species such as those in Figure 3, panel C. As expected in the solid state, **5** (5 wt % in KBr) gave corresponding bands at lower frequency: 3359, 3259, 1723, and 1622 cm^{-1}. This solid-state information allows for interpretation of the respective frequencies obtained by Raman microscopy of the assembled state. As shown in Figure 7, the bands at 1622 and 1723 cm^{-1} were assigned to the intermolecular hydrogen-bonded amide C═O and acid carbonyl, respectively.[18]

Both the NMR and IR observations with **5** are consistent with the X-ray crystallography data, which implies that the amide NH and C═O of **5** are available to form intermolecular bonds. We speculate that the "twisted" conformation of **5** (Figure 3) is favored in both the crystal state and upon solvation of **5** in $CDCl_3$. Access to this packable conformer is likely critical to the supramolecular assembly of **5** in water. To better understand the conformational preferences of these systems, we have initiated molecular modeling studies of **5** and other 1,1-disubstituted cycloalkane platforms (e.g., **3**). The modeling results along with the X-ray crystal structure of **3** are still in progress and will be reported in due course.

Conclusions

Studies of the cyclobutane diamide diacid **5** revealed the formation of solid microspheres by both the TEM and XRM techniques. The XRM experiments also revealed the formation of rodlike structures during the aqueous assembly of **5**. Single-crystal X-ray crystallography revealed that **5** packs in an extended helical array comprised of two types of intermolecular hydrogen bonds (i.e., OC═O···HN and COOH···O═CN). VT-NMR and IR measurements of **5** revealed the small temperature dependence of the amide NH chemical shift ($\Delta\delta/\Delta T = -1.1$ ppb/K) and the availability of the amide NH of **5** to form intermolecular hydrogen bonds in $CDCl_3$. Raman microscopy confirmed that nearly identical bonding patterns are present in the assembled microsphere and the crystal architecture of **5**.

It is clear that **5** is capable of forming intermolecular hydrogen bonds not only in its crystal state but also in the presence of solvents such as $CDCl_3$ and during its self-assembly in water. Collectively, these observations provide compelling evidence that the aqueous assembly of **5** occurs via supramolecular crystalline intermediates, which are similar in shape and have complementary bonding motifs for molecular recognition.

A priori one may have expected the recrystallization event to select for a particular motif, **3** or **5**. We speculate that the microsphere-building process of **5** is not capable of distinguishing between **3** and **5**, which differ only by a single CH_2 group. However, the microcapsule-forming process seems to require greater "molecular fidelity" to attain its final architecture. Such observations are critical to furthering our understanding of which factors direct molecular recognition events between peptides in aqueous environments.[3,5−7]

One outcome from these studies is that appropriately spaced "twisted" amide motifs as seen with **5** may make excellent recognition elements for COOH groups. Another logical extension of these findings is that the structure of microcrystalline domains may be important drivers of self-assembly processes, which involve phase-transition events. In addition, one may be able to control such "nanoconstructive" processes by designing new

(19) Gellman, S. H.; Dado, G. P.; Liang, G.; Adams, B. R. *J. Am. Chem. Soc.* **1991**, *113*, 1164−1173. (b) Dado, G. P.; Gellman, S. H. *J. Am. Chem. Soc.* **1994**, *116*, 1054−1062.

(20) Stevens, E. S.; Sugarwa, N.; Bonara, G. M.; Toniolo, C. *J. Am. Chem. Soc.* **1980**, *102*, 7048−7050. (b) Kessler, H. *Angew. Chem., Int. Ed. Engl.* **1982**, 512.

systems, which have complementary shapes and bonding patterns within their crystal architecture (e.g., "sticky" helical and sheet motifs)[13c] and are capable of undergoing a proton-induced phase transition.[5−7]

Experimental Section

General Procedures. Silica gel 60 (70−230 mesh) was purchased from Selecto-Scientific, Norcross, GA. All other reagents and starting materials were obtained from the Acros and Aldrich Chemical companies and were used without further purification except where indicated. ^{1}H NMR spectra were recorded at 200 MHz. IR and VT-NMR experiments were conducted using the guidelines described by Gung et al.[10]

TEM. Preparation of the sample for TEM study (e.g., Figure 2) involved the generation of a white suspension by combining 50 μL of 1 M citric acid and 50 μL of a 0.05 M aqueous solution of the sodium salt of the peptide (or peptides) **3** or **5**. The aqueous suspension was deposited on a carbon-coated copper grid rendered hydrophilic by glow discharging in air. After deposition, the specimen was washed with 1 drop of distilled water to remove excess salt followed by 1 drop of a 1% uranyl acetate stain. The excess liquid was blotted away with filter paper, and the suspension was allowed to air-dry. Electron micrographs of these negatively stained specimens were obtained on a Philips CM120 electron microscope at 120 kV and are shown in Figure 2.

Raman Microscopy. Raman spectra were obtained using a 632.8 nm line of an air-cooled, 6 mW He−Ne laser focused to a small region (e.g., the scan area was approximately 1 μm^2) on the surface of a microsphere generated from **5**. In general, microspheres were immobilized by vacuum-drying of the aqueous suspension generated from **5** (see Assembly Test). In this manner the sample was affixed to the glass slide for targeting purposes. Note: Air drying of the sample gave the same result. For comparison purposes, Raman scattering information was obtained on crystalline **5** (see panel b in Figure 7) and from the regions between the immobilized microspheres (data not shown). The Raman scattering spectrum acquired from these "blank" regions matched that of a control solution containing equal volumes of a 1 M aqueous citric acid solution and a 50 mM aqueous Na_2CO_3 solution in the absence of **5**.

Assembly Test. The diamide diacid **5** was tested for microsphere formation using a modification of our previously described procedure.[4,5] The bis-acid **5** (0.01 mmol) was dissolved in 0.1 mL of aqueous Na_2CO_3 (0.1 M) to give a clear solution of the sodium salt in deionized water. Equal volumes of this 0.1 M peptide solution and 1 M aqueous citric acid were mixed and shaken. Microscopic examination of the suspension generated from **5** revealed the formation of tiny spheres.

X-ray Microscopy. The white suspension was prepared as described in the TEM section and deposited on a poly(methyl methacrylate) photoresist and then covered by a silicon nitride coverslip in an air-tight cell. The sample was then placed in a sample holder which was located 1 cm away from a gold foil target and 45° from the target normal in a vacuum chamber. The chamber was evacuated, and a plasma was produced by irradiating the gold target with a 5 ns pulse of 1064 nm light at 20 J from a Nd:glass laser, allowing the sample to be irradiated by "soft" X-rays ($\lambda = 2-4$ nm).[8] The sample was then taken from the chamber, and the photoresist was then washed with NaOCl and developed in 50% methyl isobutyl ketone/isopropyl alcohol for 1 min. The dimensional relief obtained was imaged using a TMX 2000 Discoverer scanning probe microscope. The data are plotted in height units reflecting the height in which the cantilever tip was raised and lowered as it scanned across the surface of the resist.

X-ray Crystallography. Crystals suitable for a single-crystal X-ray diffraction study were grown by combining part of a 100 mM acetone solution of the diacid with a 1:1 toluene/diethyl ether solution (so that the total volume ratios were 1:1:1, respectively), followed by controlled evaporation of Et_2O and Me_2CO. A crystal of approximate dimensions 0.26 × 0.18 × 0.16 mm^3 was mounted under Paratone-8277 on a glass fiber and immediately placed in a cold nitrogen stream at −80 °C on the X-ray diffractometer. The X-ray intensity data were collected on a standard Siemens SMART CCD area detector system equipped with a normal focus molybdenum-target X-ray tube operated at 2.0 kW (50 kV and 40 mA). A total of 1321 frames of data (1.3 hemispheres) was collected using a narrow frame method with scan widths of 0.3° in ω and exposure times of 60 s/frame using a detector-to-crystal distance of 5.09 cm (maximum 2θ angle of 56°). The total data collection time was approximately 26 h. Frames were integrated to 46.5° with the Siemens SAINT program; however, refinement was carried out on data to 41.6° due to lack of observed data greater than that value. There was a total of 14 117 reflections collected in this range, of which 2813 were independent ($R_{int} = 4.66\%$)[21] and 2668 were observed ($>2\sigma(I)$). Laue symmetry revealed a hexagonal crystal system, and the final unit cell parameters (at −80 °C) were determined from the least-squares refinement of three-dimensional centroids of 7800 reflections.[22] Data were corrected for absorption with the SADABS[23] program.

The compound crystallized in the enantiomorphous set of space groups $P6_1$ or $P6_5$. The space group $P6_5$ was assigned, which gave the enantiomorph (L configuration) required by the synthetic procedure. The structure was solved by using direct methods and refined employing full-matrix least-squares on F^2 (Siemens, SHELXTL,[24] version 5.04). For a Z value of 6, there is one molecule in the asymmetric unit. One of the phenyl rings (C19−C24) exhibits a serious disorder, whereby two different orientations of the ring can be seen. Refinement of the SOFs (site occupancy factors) of the two different rings revealed a 60:40 occupancy ratio for the phenyl rotamer. All of the non-hydrogen atoms were refined with anisotropic thermal parameters. Acceptable anisotropic refinement of the disordered phenyl ring was made possible by using the PART instruction in SHELXL coupled with a variable-metric rigid group refinement of both rings. Hydrogen atoms were included in ideal-

(21) $R_{int} = \sum|F_o^2 - F_o^2(\text{mean})|/\sum[F_o^2]$.

(22) It has been noted that the integration program SAINT produces cell constant errors that are unreasonably small, because the systematic error is not included. More reasonable errors might be estimated at 10 times the listed value.

(23) The SADABS program is based on the method of Blessing. See: Blessing, R. H. *Acta Crystallogr., Sect. A* **1995**, *51*, 33.

(24) *SHELXTL: Structure Analysis Program*, version 5.04; Siemens Industrial Automation Inc.: Madison, WI, 1995.

Table 1. Summary of Crystallographic Data for 5

crystal data	
chemical formula	$C_{24}H_{26}N_2O_6$
formula weight	438.47
crystal system	hexagonal
space group (no.)	$P6_5$
Z	6
a, Å	22.3876(7)
c, Å	9.4793(4)
volume, Å^3	4114.5(3)
ρ_{calc}, g·cm^{-3}	1.062
temp, °C	−80
GOF[a]	1.140
$R_1(F_o)$, $wR_2(F_o^2)$ obs,[b] %	7.23, 20.38

[a] GOF = $[\sum[w(F_o^2 - F_c^2)^2]/(n - p)]^{1/2}$, where n and p denote the number of data and parameters. [b] $R_1 = (\sum||F_o| - |F_c||)/\sum|F_o|$; $wR_2 = [\sum[w(F_o^2 - F_c^2)^2]/\sum[w(F_o^2)^2]]^{1/2}$, where $w = 1/[\sigma(F_o^2) + (aP)^2 + bP]$ and $P = [(\text{Max};0,F_o^2) + 2F_c^2]/3$.

ized positions. The crystal parameters and final residuals are provided in Table 1. Complete tables of crystal data and structure refinement, atomic coordinates, bond lengths and angles, anisotropic displacement parameters, and fixed hydrogen coordinates can be found in the Supporting Information (Tables SI−SV).

Bis(N^{α}-amido-L-phenylalanine)-1,1-cyclobutane Dicarboxylate (5). The bis(*tert*-butyl) ester **6** (2.2 g, 4.0 mmol) was dissolved in $CHCl_3$ (15 mL) and cooled to 0 °C. TFA(10 mL) was added dropwise under a nitrogen atmosphere. After 2 h the volatiles were removed under reduced atmosphere to give a white foam. Recrystallization (50% hexane/ethyl acetate) provided the pure bis-acid **5** (0.55 g, 31%). ^{1}H NMR (CD_3OD): δ 7.2 (m, 10H, aromatic), 4.65 (q, 2H, CH), 3.2 (m, 2H, CH_2), 2.95 (m, 2H, CH_2), 2.3 (t, 4H, cyclobutyl), 1.7 (m, 2H, cyclobutyl). Optical rotation: $[\alpha]^{27}_D = -7°$ (c = 1.5, MeOH). Anal. Calcd for $C_{24}H_{26}N_2O_6$: C, 65.74; H, 5.98; N, 6.39. Found: C, 65.50; H, 6.06; N, 6.31.

Bis(N^{α}-amido-L-phenylalanine *tert*-butyl ester)-1,1-cyclobutane Dicarboxylate (6). Under an inert atmosphere of dry nitrogen, 1,1-cyclobutanedicarboxylic acid (1.17 g, 8.14 mmol) was dissolved in 5 mL of thionyl chloride. The clear solution was refluxed for 2 h, and the excess thionyl chloride was removed under reduced pressure. [Note: trace amounts of thionyl chloride were removed by adding and distilling out dry benzene under reduced pressure to give the crude acid chloride.] The acid chloride was dissolved in chloroform and cooled to 0 °C. In a separate step, L-phenylalanine *tert*-butyl ester hydrochloride (4.2 g, 16.3 mmol) was dissolved in $CHCl_3$ and washed with a saturated aqueous Na_2CO_3 solution. The organic layer was separated, dried over anhydrous $MgSO_4$, filtered, and concentrated to give the free amine as an oil (3.55 g, 98%). The amine was redissolved in $CHCl_3$ (25 mL) and added dropwise to the cooled acid chloride solution, along with 3 mL of diisopropylethylamine. The reaction was warmed to room temperature and stirred overnight. The solution was washed successively with 1 N HCl, water, aqueous $NaHCO_3$, and water. The organic layer was separated, dried over anhydrous $MgSO_4$, filtered, and concentrated to give a white crystalline solid. Recrystallization from 40% hexane/ethyl acetate provided the diamide **6** (2.2 g, 50% overall). ^{1}H NMR ($CDCl_3$): δ 7.30 (m, 10H, aromatic), 6.65 (d, 2H, NH), 4.65 (q, 2H, CH), 3.06 (d, 4H, CH_2), 2.45 (t, 4H, cyclobutyl), 1.9 (m, 2H, cyclobutyl), 1.5 (s,-18H, *tert*-butyl). IR (KBr): 3274, 3060, 2964, 2921, 2857, 1723, 1643, 1531, 1451, 1365, 1306, 1264, 1157 cm^{-1}. IR ($CDCl_3$, 1 mM): 3423, 3338, 2974, 2932, 1723, 1670, 1499, 1451, 1365, 1253, 1152 cm^{-1}. Optical rotation: $[\alpha]^{27}_D = 21°$ (c = 2, $CHCl_3$). Anal. Calcd for $C_{32}H_{42}N_2O_6$: C, 69.79; H, 7.69; N, 5.09. Found: C, 69.68; H, 7.69; N, 5.01.

Acknowledgment. The authors thank Dr. Raymond J. Bergeron at the Department of Medicinal Chemistry, University of Florida, for providing an authentic sample of **3** for comparison purposes. The authors also appreciate the financial support from the National Science Foundation in the purchase of our 200 MHz NMR instrument (Grant CHE-8608881). J.L. was supported by NIH Grant AR42872. The Philips CM120 was purchased with funds from the Markey Charitable Trust.

Supporting Information Available: Tables of crystal data, structure refinement, atomic coordinates, bond lengths and angles, and anisotropic displacement parameters for **5**. ORTEP of **5** showing disorder (i.e., the alternative position of the phenyl ring). Raman spectrum of the nonmicrosphere-containing regions as observed by the Raman microscope. This material is available free of charge via the Internet at http://pubs.acs.org.

CM0006547